Bulletin of the Seismological Society of America, Vol. 86, No. 6, pp. 1724–1732, December 1996

On the Coherence of Ground Motion in the San Fernando Valley

by S. E. Hough and E. H. Field

Abstract We present an analysis of the coherence of seismic ground motion recorded on alluvial sediments in the San Fernando Valley, California. Using aftershocks of the 17 January 1994 M_w6.7 earthquake recorded at a quasi-dense array of portable stations, we analyze the coherence of three well-recorded magnitude 3.7 to 4.0 events over the frequency range 0.5 to 15 Hz and a distance range of 0.5 to 5.3 km. All stations are located at sites with broadly similar near-site geology, characterized by medium to fine-grain Quaternary alluvial sediments. On average, relatively high values of coherence are observed for distances up to 3 to 4 km and frequencies up to 2 to 3 Hz; coherence drops sharply at frequencies near and above 3 Hz. Although average coherence functions are described reasonably well by a log-linear relationship with frequency, the curves at all distances exhibit a flattening at low frequencies that is not consistent with previous observations of coherence at hard-rock sites. The distance decay of coherence is also markedly less strong, with high coherence values observed over station separations corresponding to multiple wavelengths. This may reflect fundamental differences in shallow-wave propagation in the two environments, with high-frequency scattering relatively more dominant in regions of hard-rock near-surface geology. Within a sedimentary basin or valley, the site response itself generally reflects a resonance phenomenon that may tend to give rise to more uniform ground motions. However, previous studies have demonstrated the existence of pathological focusing and amplification effects within complex sedimentary basin environments such as the greater Los Angeles region; our results undoubtedly do not quantify the full range of ground-motion variability at all sites, but rather represent the level of that variability that can be expected, and quantified, for typical source/receiver paths.

Introduction

Two weeks after the M_w 6.7, 17 January 1994 Northridge earthquake, approximately 20 portable digital seismic instruments were installed in a 4-km aperture ("quasi-dense") array within the San Fernando Valley, just north of the mainshock epicenter (Mori, 1994; Fig. 1). These instruments consisted of both GEOS recorders, deployed by the United States Geological Survey (Borcherdt *et al.,* 1985), and RefTeks, deployed by institutions comprising the Southern California Earthquake Center (SCEC; Archuleta, 1994). Each GEOS site was instrumented with a three-component Mark Products L-22 2-Hz sensor and a Kinemetrics force-balance accelerometer (FBA). SCEC sites were instrumented with a variety of sensors, most having a low–high gain or strong–weak motion configuration. The GEOS and Reftek data are sampled at 200 and 250 samples, respectively, on all channels. The purpose of this array was to investigate the small-scale variability of ground motions.

The array was operated for a period of approximately 2 weeks, during which time approximately 25 events with magnitudes 2.5 to 4.0 were well recorded across the array. Events were associated with the Southern California Seismic Network (SCSN) catalog, and we will refer to the SCSN-determined local magnitudes. Most of the events were too small to generate significant lower-frequency (i.e., 1 to 3 Hz) energy. We will focus on three largest events, including two of the largest recorded aftershocks: an M4 event that occurred at 12:59 GMT on Julian day 056 (event 1; see Fig. 1) and an M3.7 event that occurred at 13:56 GMT, also on day 56 (event 2). We will also analyze the largest event that occurred within the perimeter of the array itself, an M3.7 event that occurred at 09:13 GMT on day 049 (event 3). Events 1 and 2 occurred approximately 15 km from the center of the array; event 3 occurred approximately 3.5 km from the array center. The array recorded usable FBA data at 7, 13, and 10 stations, respectively.

Because the events are fairly close to the array, some degradation in coherence may be expected to result from different sampling on the focal sphere for each event–station pair. For example, event 3 is inferred to be on the mainshock rupture plane, with a similar mechanism to the mainshock

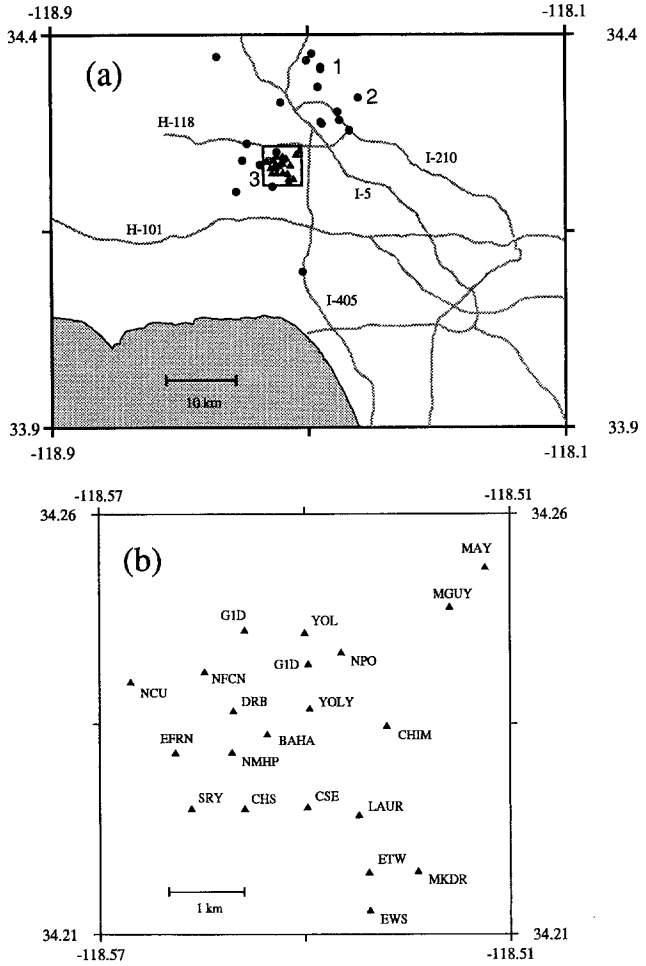

Figure 1. (a) Map of the Northridge region, including quasi-dense array stations (triangles), events recorded by array (circles), events analyzed in this study (numbered circles), and Los Angeles metropolitan-area freeways. (b) Dense array deployment of portable digital instrumentation. Stations are shown with triangles and three- or four-letter codes three-letter names correspond to GEOS recorders; four-letter names to RefTek sites).

(L. Seeber, personal comm.), and to the immediate west of the central part of the array. The array stations may thus not fall in a similar region of the *S*-wave radiation pattern for this event. We will not attempt to "dissect" this sort of detailed dependence of coherence on detailed source characteristics, but rather to characterize the average coherence. In general, however, we note that somewhat higher coherence (over a fixed array aperture) might be expected for more distant events, because of less likelihood of significant variations in radiation pattern.

In a companion article, Field and Hough (1996), henceforth FH96, estimate average damped pseudo-velocity response spectra for the same array sites using the full set of 23 events to further investigate the variability of site response across the array. In this article, we will investigate the waveform coherence of the larger recorded events. In addition to providing insights into wave propagation within the San Fernando Valley, the extent to which ground motions are incoherent can be an important consideration in the evaluation of response of critical structures such as lifelines, bridges, and other large-scale structures (e.g., Loh and Ang, 1989).

As discussed by FH96, the near-site geology across the array is predominantly characterized by the Holocene fine-grained silt and clay layer (*Qyf*) that forms the dominant upper unit in the San Fernando Valley (Tinsley and Fumal, 1985). Some of the sites are located on an overriding layer of medium-grained sand (*Qym*), also a Holocene unit. FH96 conclude that site response is somewhat more variable among the *Qym* sites and attribute this result to the more variable properties of this geologic unit across the array. For this study, differences in response caused by fine distinctions in near-site geology are one plausible source for the degradation of coherence across the array. However, for the purposes of any broad-site classification, the two units that comprise the near-surface geology of the dense array would be given the same designation. Thus, the coherence across the quasi-dense array sites is expected to characterize ground-motion variability among sites with the same general site classification, at site spacings of 0.5 to 5 km.

We emphasize that this study (and FH96) seeks to quantify ground-motion variability at sites with characteristics that are generally average, rather than those that give rise to "pathological" site or path effects. We thus, for example, would not expect our results to characterize the extreme sorts of site/path effects observed during the Northridge earthquake at Tarzana (e.g., Spudich *et al.*, 1996) or Santa Monica (Gao *et al.*, 1996). As discussed by Gao *et al.* (1996), complicated three-dimensional site-response or focusing effects may be extremely difficult to predict in advance, since they can be extremely dependent on the precise source and receiver locations.

Analysis

We first resample the SCEC data to match the 200 samples sample rate of the GEOS instruments. Then, in order to emphasize the longer periods (at which a higher coherence is expected), we integrate the recorded seismograms to displacement. The coherence results will not depend on the choice to analyze displacement, velocity, or acceleration. We integrate to displacement primarily to better emphasize the long-period coherence across the array in Figure 3 and calculate coherence from these displacement seismograms for consistency. We use the FBA recordings because of their better long-period response characteristics; there is no need to perform an instrument correction, because the response is flat in the frequency band of interest. Once we have obtained displacement, the traces are high-pass filtered using a third-order Butterworth filter and a corner frequency of 0.1 to 0.3 Hz. The filter corner was consistent for a given event; the corner was chosen based on a subjective assessment of rel-

ative signal-to-noise ratios at longer periods. Because the filter corner frequency varies between events, the highest corner will control the lower frequency bound to which the average coherence results are considered well determined. In general, given earthquakes with magnitudes close to 4, we do not expect enough long-period energy to characterize coherence for frequencies much below 0.3 to 0.5 Hz.

We will focus on the coherence of the direct S wave rather than any more-complicated later phases, such as the converted surface waves observed by Hough *et al.* (1995). However, two of the three events exhibit waveform complexity in the early S-wave train that is suggestive of source complexity (see Fig. 2). Because these later phases are complicated by early S-wave coda from the primary arrivals, we extract a 5 to 6-sec window (consistent for each event) bracketing only the direct S-wave arrival. We find that spectral (and hence coherence) results are dominated by the direct S-wave pulse seen in Figure 3. Using windows as short as 2 to 3 sec does not result in any significant change to spectral estimates for frequencies above 0.5 Hz; some changes do result at the lowest frequencies, but, as mentioned above, we have little resolution at frequencies lower than 0.5 Hz in any case. We thus do not attempt to more narrowly window the direct S wave, to maximize the resolution at frequencies near 0.5 to 1 Hz, and to avoid subjective determination of the exact time duration of the direct wave (see, for example, the trace from station CHS, in Fig. 3). A cosine taper is applied to 5% of the time series shown in Figure 3. Once the S-wave pulse is windowed, we then align the time series (by eye) to account for propagation delays across the array.

For each horizontal component, we calculate waveform coherence for each pair of records. Although this produces nonindependent coherence results, it prevents bias caused by reliance on data from a single station as a "reference" trace. We define coherence using the standard definition

$$C(f, r) = \frac{|\langle s^*(x_1, f)s(x_2, f)\rangle|^2}{[\langle s^*(x_1, f)s(x_1, f)\rangle][\langle s^*(x_2, f)s(x_2, f)\rangle]}, \quad (1)$$

(e.g., Menke *et al.*, 1990), where $s(x_i,f)$ is the Fourier transform of the ith time series and * denotes the complex conjugate. The angular brackets indicate the ensemble average of the cross- and auto-power spectra. We calculate the spec-

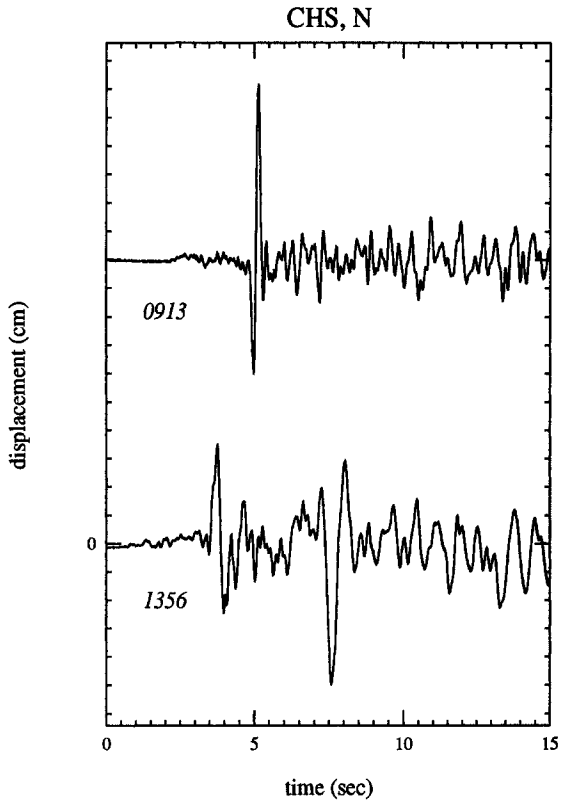

Figure 2. The north component of motion recorded at station CHS for events 2 (1356) and 3 (0913). The conspicuous late phase in the bottom record is not qualitatively consistent with inferred converted surface-wave observations by Hough *et al.* (1994) for stations in the same vicinity and may represent source complexity.

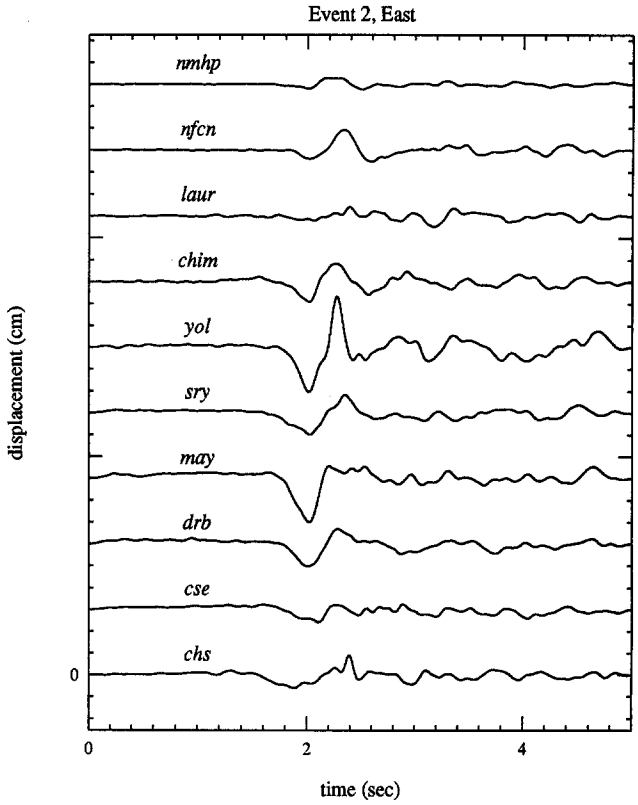

Figure 3. The E–W component of ground motion for event 2 recorded at all array sites for which good data were obtained. Acceleration records are doubly integrated and high-pass filtered above 0.1 Hz to obtain displacement. Records are offset for clarity and are aligned along the first positive pulse. Each small tic mark on the vertical axis indicates 0.02 cm.

tra using the multi-taper method (e.g., Thompson, 1982; Park *et al.,* 1987) with 4π-prolate tapers, providing an equivalent smoothing bandwidth of 0.34 Hz. This method effectively ensures spectral smoothing in a way that is optimal in a prescribed sense, optimizing the trade-off between spectral leakage and resolution (Thompson, 1982). Although this method renders redundant the preprocessing stage of the cosine taper, the results are completely insensitive (to the resolution limits that any of the subsequent results are shown) to the extra tapering.

S-Wave Coherence

In Figure 3, we show examples of *S* waves recorded across the array: displacement seismograms of event 2 from the east component at all stations that provide good data for each event. In Figure 4, we show coherence results corresponding to the seismograms shown in Figure 3, relative to station DRB. Although Figure 4 and all subsequent figures present coherence over the full- 0 to 15-Hz range, we do not, for reasons discussed above, ascribe any significance to values for frequencies below 0.5 Hz. To better visualize the full set of results, we use the plotting software GMT (Wessel and Smith, 1991) to generate "coherencegrams," in which coherence levels are displayed using a black and white or color pallet for a range of frequencies and station separations. To make these figures, we first calculate coherence for a suite of station pairs as described above; we then create a matrix of coherence values for equally spaced frequency and distance values. We choose a high-frequency cutoff of 15 Hz. The distance range is governed by the available range of station spacings: roughly 500 to 5100 m. The gridding is done using interpolation under tension, so that no minima or maxima are created away from the constrained data points (Smith and Wessel, 1990). Coherencegrams for events 1, 2, and 3 are shown in Figure 5.

It is evident from Figure 5 that the coherence results are characterized by a certain level of variability. This may reflect real differences in coherence, perhaps caused by differing levels of path complexity, as well as sources of observational uncertainty (e.g., uncertainties related to imperfect spectra resolution, imperfect time-series alignment, etc). In order to further examine the average coherence, we bin the results by station separation, using increments of 200 m (i.e., 500 to 699 m, 700 to 899 m, etc.) up to 1700 m; increments of 400 m from 1700 to 2900 m; and increments of 800 from 2900 to 5300 m. Although this binning is somewhat *ad hoc,* we will show that the coherence results are surprisingly consistent over a broad range of station separations, and so our results are not critically dependent on the ranges chosen. The average results are shown in Figure 6. Finally, we combine the results shown in Figure 6 to obtain a coherencegram for frequencies of 0 to 15 Hz and station separations of 500 to 5300 m, using the results from all events and both horizontal components (Fig. 7).

To determine the significant level of coherence, we analyzed random time series using the same approach described above. This test revealed a coherence significance threshold of approximately 0.40 (i.e., 95% of the coherence values were below this level). We thus conclude that the flattening of all coherence curves for frequencies above ≈5 Hz indicates the level at which coherence is indistinguishable from random.

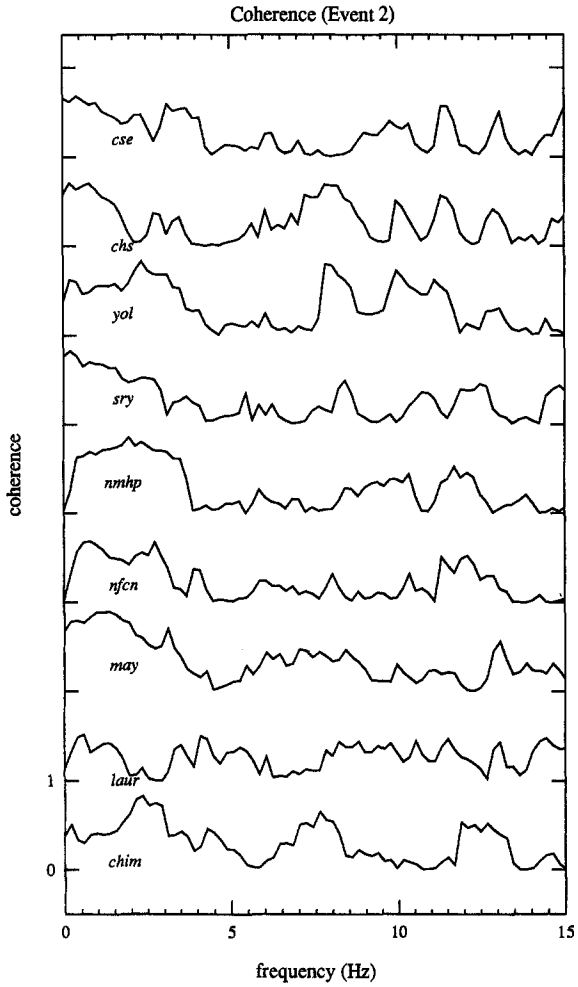

Figure 4. Coherence as a function of frequency corresponding to the seismograms shown in Figure 3, relative to station DRB. Each successive curve is offset by one unit for clarity and labeled by station; each tic mark on the vertical axis indicates 1 unit.

To examine the variability of our coherence estimates, we can calculate sample population standard deviations for the averaged results. Figure 8a shows the 1 σ standard deviation corresponding to the coherence results for 500 to 699 m; the results for the 900 to 1099-m range are shown in Figure 8b. The standard deviations observed for the individual bins are observed to be fairly large; however, Figure 6 reveals very little discernible difference in observed coherence up to approximately 3600 m. In Figure 8c, we combine all coherence observations for the distance range 500 to 3699 m; the reduced sample standard deviation indicates the consistency of our coherence results over this distance range.

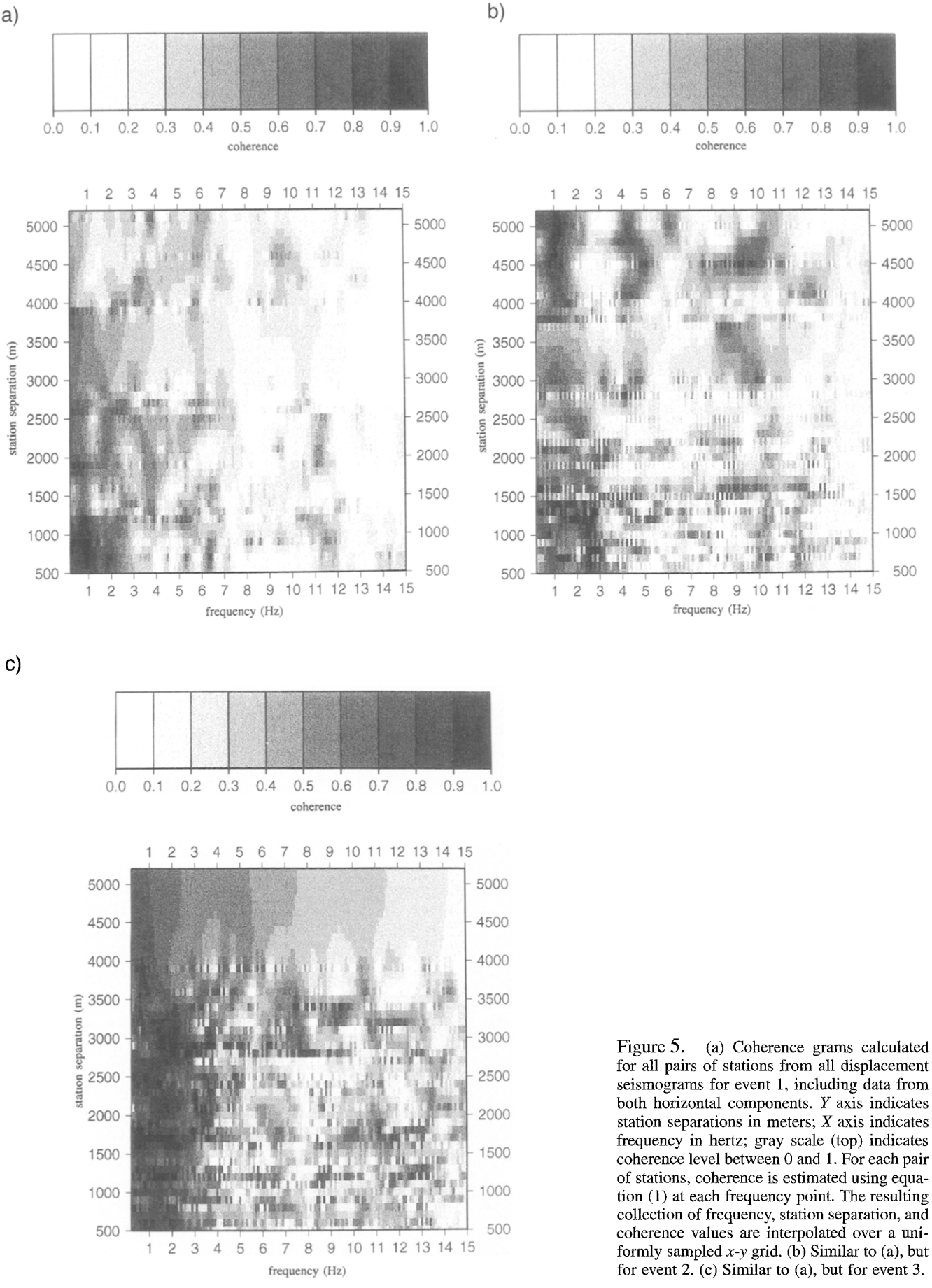

Figure 5. (a) Coherence grams calculated for all pairs of stations from all displacement seismograms for event 1, including data from both horizontal components. *Y* axis indicates station separations in meters; *X* axis indicates frequency in hertz; gray scale (top) indicates coherence level between 0 and 1. For each pair of stations, coherence is estimated using equation (1) at each frequency point. The resulting collection of frequency, station separation, and coherence values are interpolated over a uniformly sampled *x*-*y* grid. (b) Similar to (a), but for event 2. (c) Similar to (a), but for event 3.

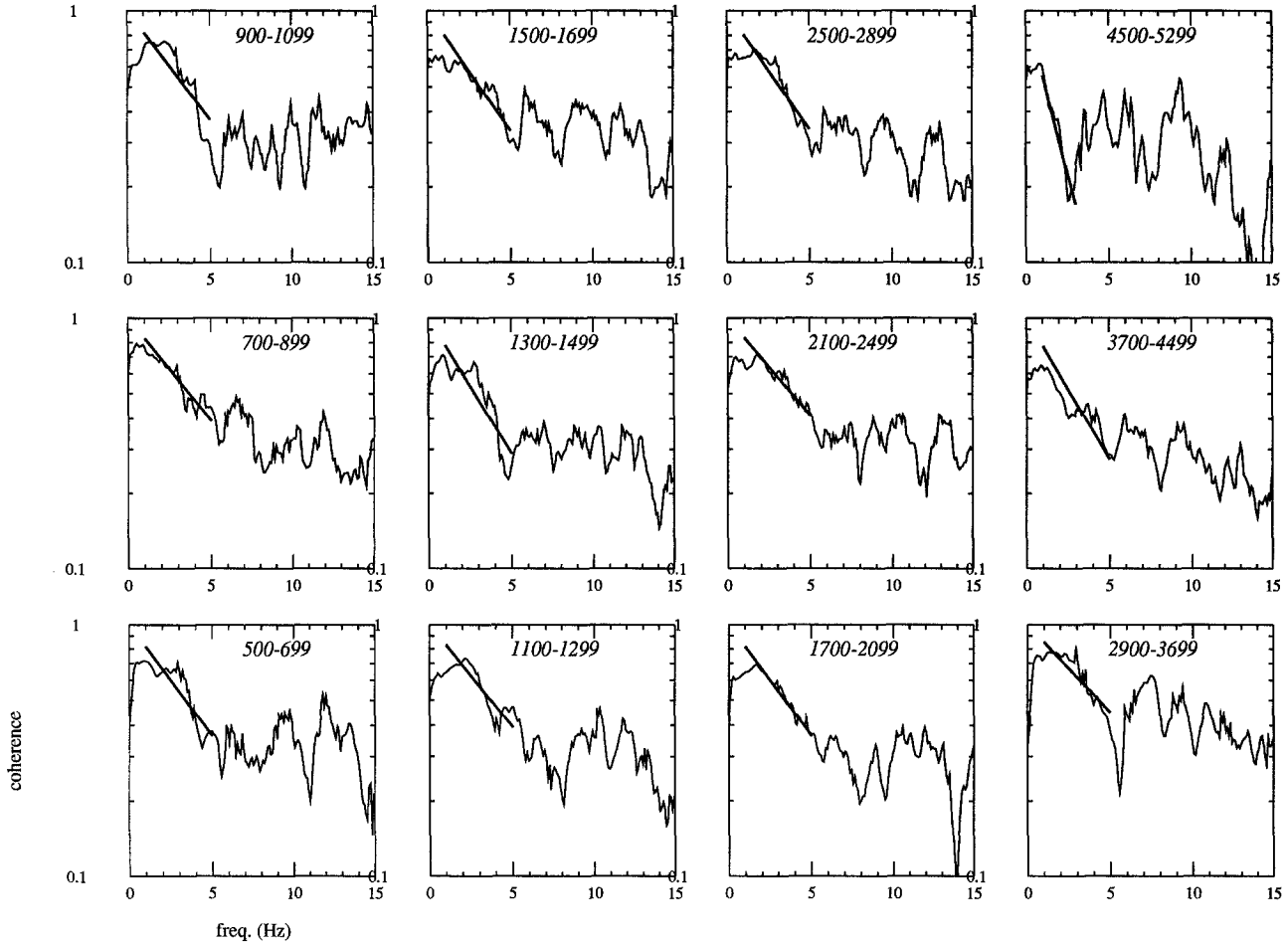

Figure 6. Coherence functions as a function of stations separation, averaged over indicated station separation bins (for all events and both horizontal components). Superimposed are best-fit exponential decay models (equation 2) to each observation.

Interpretation

Although coherence values are found to be somewhat variable, high coherence values are generally observed. At frequencies of ≈2 Hz, Figures 6 through 8 reveal average coherence coefficients of at least 0.5 for station separations as large as 3 km. These coherence values are controlled by the direct *S*-wave arrival, which generally dominates the displacement record. Vidale and Helmberger (1988) obtain *S*-wave velocities of roughly 600 to 1100 m/sec; consistent results are inferred by Hough *et al.* (1995), who use slowness analysis of Northridge aftershock data from very dense arrays to obtain apparent *S*-wave velocities of inferred converted surface waves. An average *S*-wave phase velocity of 800 m corresponds to wavelengths of roughly 800 m at 1 Hz and 400 m at 2 Hz.

Menke *et al.* (1990) showed that coherence over the frequency range 5 to 25 Hz at hard-rock sites could be modeled by

$$C(f, \delta x) = e^{-Af\delta x}, \quad (2)$$

where δx is the station separation and A is a constant. They obtain a value of A of 0.67 km^{-1} Hz^{-1}. In Figure 6, we superimpose least-squares best-fit exponential decay models to each average coherence estimate. Although the fit in each case is broadly consistent with the observations, equation (2) does not provide an overall satisfactory model: the decay of coherence with both frequency and distance is markedly less pronounced than prescribed by equation (2). In fact, up to a separation of 3600 m, the observed average coherence curves are fit by a modified version of equation (2),

$$C(f, \delta x) = e^{-A'f}, \quad (3)$$

where A' is now constant. The least-squares regressions yield an average value of $A' = 0.20$ for the 10 bins up to 3600 m, with all values within the range 0.17 to 0.25.

We note, however, that the coherence curves also exhibit a suggested flattening at the longer periods (≈1 to 3 Hz) that is not well modeled by equation (3). Coherence is, of course, expected to be 1 for 0 Hz, and so we attribute the decay of inferred coherence at the longest periods to the lack

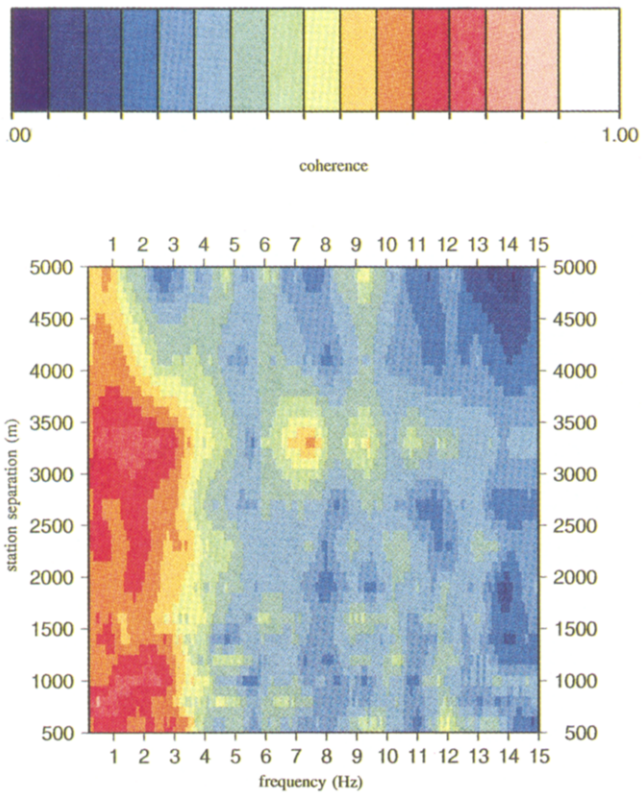

Figure 7. Coherence-gram corresponding to averaged (binned) coherence results shown in Figure 6 (see Fig. 5a caption for plotting conventions).

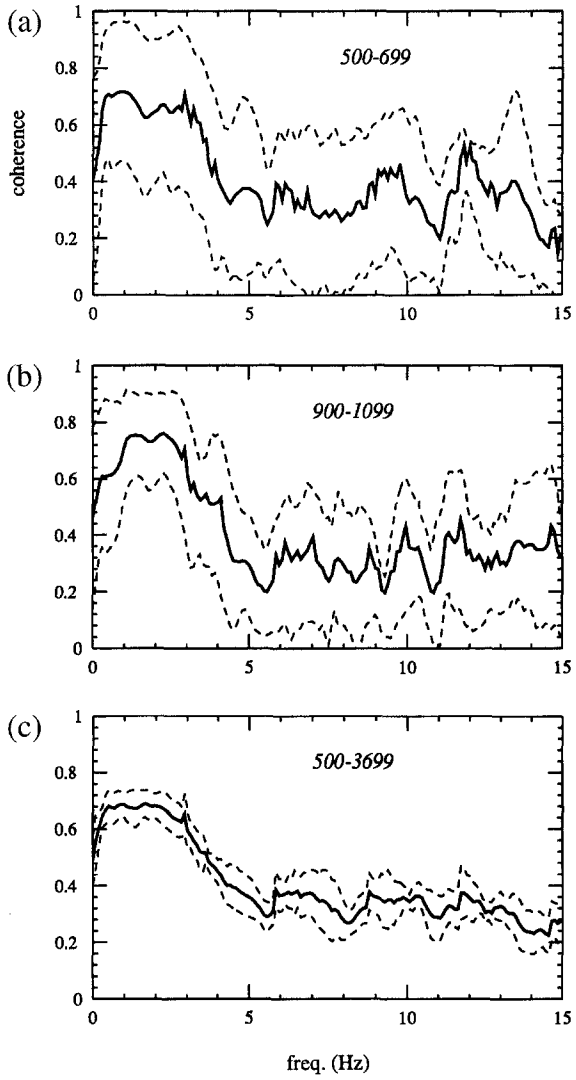

Figure 8. (a) Solid line indicates average coherence curve for station separation range of 500 to 699 m; dashed lines indicate 1 σ sample standard deviation. (b) Same as (a), except for station separation range of 900 to 1099 m. (c) Solid line indicates average coherence curve for station separation range of 500 to 3699 m; dashed lines indicate 1 σ sample standard deviation.

of sufficient long-period signal across the array. However, the analyzed events have energy predominantly in the 1- to 3-Hz frequency range, and so we cannot ascribe the flattening within this range to noise or lack of resolution.

Our results are thus inconsistent with an extrapolation of the results of Menke *et al.* (1990), who conclude that significant coherence in a hard-rock environment in the Adirondack mountains is observed only to distances of less than one wavelength for frequencies between 5 and 30 Hz. This contrast is consistent with the conclusions of Schneider *et al.* (1992), who find higher coherence at a sediment site in Taiwan than results from other hard-rock regions. However, the final average coherence curves shown in Figure 8 are quite similar to those obtained by Vernon (1989) for the most distant pair of stations (301-m spacing) comprising a dense array at Pinyon Flat (PFO): coherence values of $\approx$0.6 for frequencies below 2 to 3 Hz, declining rapidly to random levels by 5 Hz. The PFO array was located on the Pennisula Ranges batholith in southern California, in a region where significant site effects are not expected.

Schneider *et al.* (1992) concluded that coherence is more variable at rock sites; this could indicate that high-frequency scattering is relatively more important in some regions with hard-rock near-surface site geology. However, the consistency between the results from PFO and from this study also indicate that the discrepancy between our results and those of Menke *et al.* (1990) may reflect a fundamental breakdown in the extrapolation of the latter results to lower frequencies. If, as concluded by Menke *et al.* (1990), coherence decay is primarily caused by scattering in the uppermost crust (i.e., a few hundred meters), then it is reasonable to expect a transition in the character of coherence curves at wavelengths near and above the scale of the strongly scattering region. If the very near-surface (*P*-wave) velocity at the Adirondack mountain site is 2 to 3 km/sec, this transition would occur near 4 to 6 Hz if the scattering region extends to 500 m depth. It is plausible that a similar transitional frequency exists for the Northridge quasi-dense array region.

Assuming, for lack of an alternative model, the same 500-m extent of a strongly scattering region, a frequency on the order of 0.5 Hz would be predicted. Unfortunately, our results provide little constraint on coherence at frequencies below 0.5 Hz, because of the low levels of longer-period energy from moderate-sized events. Although these particular values are very poorly constrained, they serve to illustrate the inadequacy of any extrapolation of coherence results beyond the frequency range over which they are determined.

Conclusions

We have used data from three moderate aftershocks of the Northridge earthquake recorded across a quasi-dense array of 21 stations to investigate waveform coherence over 0.5- to 5-km separations. In a separate study, Field and Hough (1996) used data from the same array to show that (1) response spectra estimates across the array vary by approximately a factor of 2, and (2) given the uncertainty in response spectrum estimate at each site caused by observational uncertainties (i.e., uncertainties related to spectral resolution, alignment of time series, etc.), different positions on the focal sphere, and real event-to-event variability, the observed differences in average site response across the array are not judged to be significant. That is, it is not possible to significantly reduce the variability of site-response estimates by correcting for site-specific–response estimates.

The results presented here show that relatively high values of waveform coherence are observed at frequencies up to approximately 2 to 3 Hz and distances of 3 to 4 km. Figure 7 reveals that our average coherence results are relatively flat below both of these limits but decay quite sharply above them. Although the shape of the coherence function resembles the exponential shape proposed by Menke *et al.* (1990) for hard-rock sites, the decay with both distance and frequency is markedly less sharp. We suggest that this disparity may, in part, reflect fundamental differences in wave propagation in hard-rock versus sedimentary environments. By its very nature, propagation in large sedimentary basins and valleys generally represents a resonance effect; it is not surprising that ground motions might therefore be fairly uniform over kilometer-type distances, although, ultimately, coherence will degrade due to scattering. Speculatively, this phenomenon could be responsible for the suggested flattening of the coherence curves at frequencies of $\approx$1 to 3 Hz.

A second explanation may also explain part of the apparent difference between coherence inferred in this study and that obtained at the Adirondack hard-rock site by Menke *et al.* (1990). If, as suggested by Menke *et al.* (1990), coherence decay is strongly controlled by scattering within the upper 100 to 1000 m of the crust, then it is reasonable that coherence would be higher for wavelengths well above the typical size of the scatterers. Scattering could be due to either small-scale lateral heterogeneities or propagation complexities related to near-surface wave guides (sedimentary/weathered upper layers), since either could be characterized by a scale length that gives rise to a transitional frequency.

The waveform coherence results presented in this study support the general conclusions of Field and Hough (1996) regarding microzonation: That a site-response estimate can be considered an adequate representation of expected site response for sites up to a few kilometers away if they are characterized by similar near-site geology. We do note that the intrinsic uncertainty level associated with any such estimate is nontrivial; a factor of $\sim$2 uncertainty is observed in both response spectral estimates (Field and Hough, 1996) and simple ground-motion amplitudes, such as those shown in Figure 3. Hough *et al.* (1995) illustrate directly the qualitative ground-motion variability observed at a single site for different source locations, using data from stations within the region covered by the quasi-dense array deployment discussed here.

The above potential complexities notwithstanding, the quasi-dense array deployment was motivated by a desire to investigate directly the variability of ground motions within the type of large-scale sedimentary valley or basin that characterizes much of the greater Los Angeles region. The study was motivated in part by observations like those shown in Figure 8 and by observations of apparently capricious damage from the mainshock (e.g., Cranswick, 1994); these and other observations have raised questions regarding the extent to which detailed site and path effects can be quantified. The quasi-dense array deployment covered approximately a 5-km-square region characterized by generic alluvial site conditions, away from regions in which notably complex path or site effects had been observed (or otherwise expected). In our analysis, we have thus sought to address the question of expected ground-motion variability over the type of length scales that one might wish to microzone for seismic hazard assessment. Our results do not include the type of extreme site and path complexity that are known to have played a role in mainshock ground motions from the Northridge mainshock at a number of sites, such as the marked local amplification at the Tarzana site (Wennerberg *et al.,* 1994; Spudich *et al.,* 1996) or the significant focusing effects documented for the Santa Monica region (Gao *et al.,* 1996). However, we do not consider it feasible to incorporate such effects in microzonation efforts given existing technology, given their apparent dependence on specific source-receiver path.

Acknowledgments

We thank Jim Mori for spear-heading the array deployment, Adam Edelman for providing the data and instrument response characteristics, Jennifer Scott for her help with the RefTek data, Walter Smith for GMT tips, Paul Spudich for a thoughtful review, and two anonymous reviewers for their comments. We thank the many families who graciously allowed use of their backyards for the deployment and Bill Curtis and Darryl Baisley for their work in site permitting and installation. The Southern California Earthquake Center is supported by grants from the National Science Foundation and the United States Geological Survey.

References

Aki, K. and P. G. Richards (1980). *Quantitative Seismology,* W. H. Freeman and Co., San Francisco. (1994).

Archuleta, R. J. (1994). SCEC portable instrumentation and analysis of the source and site effects of the Northridge earthquake (abstract), *Trans. Am. Geophys. Union,* **75,** 175.

Borcherdt, R. G., J. B. Fletcher, E. G. Jensen, L. Maxwell, J. R. Van Shaak, R. E. Warrickm, E. Cranswick, J. S. Johnston, and R. McClearn (1985). A general earthquake-observation system, *Bull. Seism. Soc. Am.* **75,** 1783–1825.

Cranswick, E. (1994). Damage done by the 1994 Northridge, California, earthquake and the spatial density of sampling strong ground motion (abstract), *Seism. Res. Lett.* **65,** A54.

Field, E. H. and S. E. Hough (1996). The variability of PSV Response Spectra across the San Fernando dense array deployed during the Northridge aftershock sequence, submitted, *Earthquake Spectra.*

Frankel, A., S. Hough, P. Friberg, and R. Busby (1991). Observations of Loma Prieta aftershocks from a dense array in Sunnyvale, California, *Bull. Seism. Soc. Am.* **74,** 1900–1922.

Frankel, A. and J. Vidale (1992). A three-dimensional simulation of seismic waves in the Santa Clara Valley, California, from a Loma Prieta aftershock, *Bull. Seism. Soc. Am.* **82,** 2045–2074.

Frankel, A., S. Hough, G. Glassmoyer, E. Sembera, C. Dietel, and L. Hwang (1992). Seismic response of the San Bernardino Valley to Landers-Big Bear aftershocks: implications for seismic hazard to buildings (abstract), *Trans. Am. Geophys. Union* **73,** 382.

Gao, S., H. Liu, P. M. Davis, and L. Knopoff (1996). Localized amplification of seismic waves and correlation with damage due to the Northridge earthquake: evidence for focusing in Santa Monica, *Bull. Seism. Soc. Am.* **86B,** S209–S230.

Hough, S. E., C. Dietel, G. Glassmoyer, and E. Sembera (1995). On the variability of aftershock ground motions in the San Fernando Valley, *Geophys. Res. Lett.* **22,** 727–730.

Loh, C. H. and A. H.-S. Ang (1989). Stochastic seismic response sensitivity of lifeline systems, in *Structural Safety and Reliability 1,* A.H.-S. Ang, M. Shinozuka, and G. I. Schueller (Editors), American Society of Civil Engineers, New York, 677–684.

Menke, W., A. Lerner-Lam, B. Dubendorff, and J. Pacheco (1990). Polarization and coherence of 5 to 30 Hz seismic wave fields at a hard-rock site and their relevance to velocity heterogeneities in the crust, *Bull. Seism. Soc. Am.* **80,** 430–449.

Mori, J. (1994). U.S. Geological Survey response to the Northidge, California earthquake, *Trans. Am. Geophys. Union* **75,** 175.

Park, J., C. Lindberg, and F. L. Vernon III (1987). Multitaper spectral analysis of high-frequency seismograms, *J. Geophys. Res.* **92,** 12675–12684.

Smith, W. H. F. and P. Wessel (1990). Grading with continuous curvature splines in tension, *Geophysics* **55,** 293–305.

Schneider, J. F., N. A. Abrahamson, and J. C. Stepp (1992). The spatial variability of earthquake ground motion and effects of local site conditions, in *Proc. 10th World Conference Earthquake Eng.,* July 19–24, Madrid, Spain.

Spudich, P., M. Hellweg, and W. H. K. Lee (1996). Directional topographic site response at Tarzana observed in aftershocks of the 1994 Northridge, California, earthquake: implications for mainshock motions, *Bull. Seism. Soc. Am.* **86B,** S193–S208.

Thompson, D. J. (1982). Spectrum estimation and harmonic analysis, *IEEE Proc.* **70,** 1055–1096.

Tinsley, J. C. and T. E. Fumal (1985). Mapping Quaternary sediment deposits for areal variations in shaking response, Ziony and Kockelman (Editors), *U.S. Geol. Surv. Profess. Pap. 1360,* 101–126.

Vernon, F. L. (1989). Analysis of data recorded at the ANZA seismic network, *Ph.D. Thesis,* University of California at San Diego, 191 pp.

Vidale, J. E. and D. V. Helmberger (1988). Elastic finite-difference modeling of the 1971 San Fernando, California, earthquake, *Bull. Seism. Soc. Am.* **78,** 122, 141.

Wennerberg, L., R. D. Borcherdt, C. Mueller, C. Dietel, E. Sembera, and R. Westerlund (1994). Aftershock observations suggestive of large, linear site amplification at the Cedar Hill nursery accelerograph station, Tarzana, California (abstract), *Seism. Res. Lett.* **65,** A56.

Wessel, P. and W. H. F. Smith (1991). Free software helps map and display data, *Trans. Am. Geophys. Union* **441,** 445–446.

United States Geological Survey
Pasadena, California 91106
(S.H.)

Southern California Earthquake Center
Los Angeles, California 94035
(E.F.)

Manuscript received 12 October 1995.